

INVESTIGATION ON THE CHINOOK OPERATIONS WITH AN EXTERNAL SLUNG LOAD AFTER CABLE FAILURE

Reinier van der Kamp
TU Delft, The Netherlands
Ton Schattorie
Royal Netherlands Air Force

Marilena D. Pavel
TU Delft, The Netherlands
Robert le Fevre
TNO, The Netherlands

Abstract

Within The Royal Netherlands Air Force (RNLAf), the Chinook tandem helicopter with external slung load is one of the most active operating helicopters, being employed in both military and humanitarian actions. Up to the present, during RNLAf operations with Chinooks, every large external load was underslung by means of a two-strop suspension system backed up by a third point of suspension called 'redundant HUSLE' (i.e. a redundant set of slings which come into action if one of the normal strops fails). The redundant HUSLE is known to be quite expensive in terms of time and operating costs. Therefore the question arose whether it would be safely enough to replace the three-point suspension system by a two-point suspension system, eliminating the redundant HUSLE. The goal of the present paper is to investigate the behaviour of a Chinook helicopter with external slung load following the premature breakdown of one of its cables sustaining the slung load and check whether the three-point suspension system can be safely replaced by a two-point suspension. For this, a simulation model representing the flight dynamics of a Chinook CH47-B helicopter carrying a suspended load in inverted V-suspension was developed and used to fly different failure scenarios in two-and-three-point suspension. The paper will show that although in general flying with the redundant HUSLE results in less violent helicopter reactions in case of cable failure, redundant HUSLE does not necessarily mean safer. It could be concluded that flying with loads up to at least 2000 kg could be safely done in a two-point suspension system, eliminating thus the redundant HUSLE.

Notations

a_0 Blade cone flapping angle constant over the azimuth angle [rad]
 a_1 Blade longitudinal flapping angle, positive for rotor disc plane pointing backward [rad]

b_1 Blade lateral flapping angle, positive for rotor disc plane pointing in the direction of 90° azimuth [rad]
 C_D Blade drag coefficient [-]
 C_{D0} Zero thrust blade drag coefficient [-]
 C_{damp} Sling damping coefficient [-]
 C_{Dt} Blade drag coefficient with respect to thrust coefficient [-]
 C_{FE} Flat plate drag coefficient of helicopter and load body [-]
 C_H Rotor horizontal force coefficient [-]
 C_S Rotor lateral force coefficient [-]
 C_l^α Blade lift slope [1/rad]
coll Collective pilot control input, positive for increased thrust [cm]
 C_Q Shaft torque coefficient [-]
 $C_{Tf,r}$ Front and rear rotor thrust coefficient [-]
 $C_{TGl,f,r}$ Front and rear rotor thrust coefficient determined with Glauert theory [-]
 $C_{Y\beta}$ Body force sideslip lift slope in y-direction [1/rad]
 dV_{ij} Relative velocity between the endpoints of sling ij [m/s]
 f_1 Distance between helicopter plane of symmetry and helicopter centre of gravity in helicopter y-direction [m]
 $fs_{1,2,3}$ Distance between helicopter suspension points and helicopter body axes system in x-direction [m]
 $F_{x,y,z}$ All forces on the helicopter in the helicopter system, gravity not included [N]
 g Gravitational acceleration [m/s^2]
 h_{cgl} Distance between load centre of gravity and top of the load [m]
 $h_{f,r}$ Distance between rotor hub and helicopter body axes system in z-direction [m]
 h_l Load height [m]
 $hs_{1,2,3}$ Distance between helicopter suspension points and helicopter body axes system in z-direction [m]
 $H_{xf,r}$ Horizontal drag force on rotor hub in rotor disc plane [N]

Paper presented at the 31st European Rotorcraft Annual Forum, Florence, Italy, September 13-15, 2005

$H_{Yf,r}$	Lateral force on rotor hub in helicopter body axes system, in the direction of 90° azimuth [N]	p	Angular velocity around local x-axis [rad/s]
I	Mass moment of inertia [kg m^4]	pedal	Directional pilot control input, positive for right pedal pushed [cm]
$i_{f,r}$	rotor incidence angle [rad]	q	Angular velocity around local y-axis [rad/s]
I_β	Blade moment of inertia around flapping hinge [m^4]	R	Rotor radius [m]
k	cable stiffness of the slings between helicopter and load [m]	r	Angular velocity around local z-axis [rad/s]
K_a	Local aerodynamic force on the blade [N]	r_b	radius on rotor blade [m]
k_p	Lateral control gain for derivative roll control [cm-s/rad]	R_{b-g}	Rotation matrix from global coordinates to helicopter body coordinates [-]
k_q	Longitudinal control gain for derivative pitch control [cm-s/rad]	R_l	Rotor inflow angle factor [-]
k_r	Directional control gain for derivative pedal control [cm-s/rad]	R_{l-g}	Rotation matrix from global coordinates to load coordinates [-]
k_{yint}	Directional control gain for integrator pedal control [cm/(rad-s)]	S	Force on slings [N]
k_z	Collective control gain for proportional height control [-]	$S_{damp,ij}$	Damping force in the direction of sling ij [N]
k_{zflux}	Collective gain for derivative height control [s]	S_u	Force on upper sling of Y-shaped suspension [N]
k_{zint}	Collective control gain for integrator height control [1/s]	T	Thrust [N]
k_ϕ	Lateral control gain for proportional roll control [cm/rad]	u	Velocity in local x-axis [m/s]
$k_{\phi int}$	Lateral control gain for integrator roll control [cm/(rad-s)]	U_P	Local velocity on the blade perpendicular to the shaft axis [m/s]
k_θ	Longitudinal control gain for proportional pitch control [cm/rad]	U_T	Local tangential velocity on the blade [m/s]
$k_{\theta int}$	Longitudinal control gain for integrator pitch control [cm/(rad-s)]	v	Velocity in local y-axis [m/s]
k_ψ	Directional control gain for proportional pedal control [cm/rad]	V	Velocity [m/s or knots]
L	Moment in local x-direction [Nm]	w	Velocity in local z-axis [m/s]
l_{oij}	Zero tension length of sling ij [m]	w_{cgl}	Distance between load centre of gravity and right side of the load [m]
lateral	Lateral pilot control input, positive to the right [cm]	w_l	Load width [m]
l_{cgl}	Distance between load centre of gravity and front side of the load [m]	X	All forces including gravity on the helicopter centre of, in helicopter x-direction [N]
$l_{f,r}$	Distance between rotor hub and helicopter body axes system in x-direction [m]	X_B	Aerodynamic force on helicopter, in helicopter x-direction [N]
l_{ij}	Length of sling ij [m]	$X_{Rf,r}$	Front and rear rotor forces in helicopter x-direction [N]
l_l	Load length [m]	X_S	All sling forces in helicopter x-direction [N]
long	Longitudinal pilot control input, positive forward [cm]	y	y-coordinate [m]
$L_{Qf,r}$	Torque of the front and rear rotor in body x-direction [Nm]	Y	All forces including gravity on the helicopter centre of gravity, in helicopter y-direction [N]
m	Helicopter mass[kg]	Y_B	Aerodynamic force on helicopter, in helicopter y-direction [N]
M	Moment in local y-direction [Nm]	$Y_{Rf,r}$	Front and rear rotor forces in helicopter y-direction [N]
M_a	Aerodynamic moment of the blades on rotor shaft [Nm]	Y_S	All sling forces in helicopter y-direction [N]
$M_{Qf,r}$	Rotor torque in shaft axis [Nm]	z	z-coordinate [m]
N	Moment in local z-direction [Nm]	Z	All forces including gravity on the helicopter centre of, in helicopter z-direction [N]
$N_{Qf,r}$	Torque of the front and rear rotor in body z-direction [Nm]	Z_B	Aerodynamic force on helicopter on z-axis [N]
		$Z_{Rf,r}$	Front and rear rotor forces in z-direction [N]
		Z_S	All sling forces in helicopter z-direction [N]
		α	Angle of attack [rad]
		α_{ij}	Angle between helicopter X-axis and sling ij, positive in Y direction [rad]
		α_{ij}	Angle between load X_l -axis and sling ij, positive in Y_l direction [rad]
		β	Sideslip angle [rad]
		β	Blade flapping angle [rad]

β_{ij}	Angle between helicopter Z-axis and sling ij [rad]
β_{lij}	Angle between load negative Z _l -axis and sling ij [rad]
ϕ	Bank angle [rad]
λ_0	non-dimensional uniform induced downwash of the rotor [-]
$\mu_{xf,r}$	Front and rear rotor advance ratio in helicopter x-direction [-]
$\mu_{yf,r}$	Front and rear rotor advance ratio in helicopter y-direction [-]
$\mu_{zf,r}$	Front and rear rotor advance ratio in helicopter z-direction [-]
θ	Attitude angle [rad]
$\theta_{of,r}$	Collective control angles at the rotor hubs [rad]
$\theta_{1cf,r}$	Lateral control angles at the rotor hubs [rad]
$\theta_{1cf,r,pilot}$	Lateral control angles at the rotor hubs before β -correction is applied [rad]
$\theta_{1sf,r}$	Longitudinal control angles at the rotor hubs [rad]
$\theta_{1sf,r,pilot}$	Longitudinal control angles at the rotor hubs before β -correction is applied [rad]
θ_{twist}	Blade twist angle [rad]
ρ	Air density [kg/m ³]
σ	Rotor solidity [-]
τ	Time delay [s]
Ω	Rotor angular velocity [rad/s]
Ψ	Yaw angle [rad]
ψ	Rotor blade azimuth angle [rad]

Indices

1sec	At 1 second after failure
2sec	At 2 seconds after failure
b	Helicopter body coordinates
b1-3	First to third component of a vector, which is in helicopter body coordinates
C	Sling forces and moments on the load
cg_H	Helicopter centre of gravity
cg_L	Load centre of gravity
cp	Connection Point, the endpoint of a sling
f	Front rotor hub
fus	Helicopter fuselage
H	Horizontal hub forces
i	Helicopter suspension point number fore/aft
j	Suspension point number at helicopter
	Suspension point i, 1 for right and 2 for left
l	Load coordinates
l1-3	First to third component of a vector, which is in load coordinates
r	Rear rotor hub
R	Rotor hub forces
req	Required
S	Sling forces and moments on the helicopter
sl	Sling load

SPH	Suspension Point underneath the Helicopter
SPL	Load suspension point

Abbreviations

ADS	Aeronautical Design Standard
AFCS	Aircraft Flight Control System
BOL	Begin-Of-Life
EOL	End-Of-Life
HQs	Handling qualities
HUSLE	Helicopter Underslung Load Equipment
PID	Proportional, Integrator, Derivative control
red	redundant
RNLAF	Royal Netherlands Air Force
SP	Suspension Point

Introduction

One of the major helicopter attributes is its ability to transport cargo externally in the form of external slung loads. However, transporting external loads can sometimes lead to dangerous situations endangering the safety of the helicopter and its crew. The problem addressed in this paper concerns the behaviour of a helicopter following the premature breakdown of one of its cables sustaining the slung load. As helicopter example, the paper will consider the Chinook helicopter CH-47B with an external load. The variant CH-47D helicopter is actively operating within the Royal Netherlands Air Force (RNLAF) being used for both military and humanitarian operations. Up to the present, during RNLAF operations with Chinooks, every large external load was underslung by means of a three-strop suspension system, i.e. a two-strop suspension backed up by a third point of suspension, the so-called 'redundant HUSLE'. A redundant HUSLE is actually a redundant set of slings which come into action if one of the normal strops fails (see Fig. 1, right hand side).

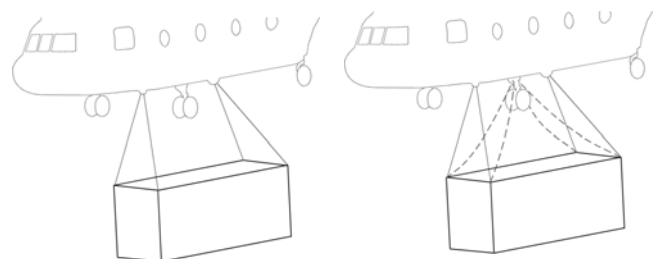


Fig. 1: Two-and-Three point suspension of the slung load

However, such a system is expensive in terms of both money and time. The question arose whether the three-point suspension system could be safely replaced by a two-point suspension. In other words, the question was posed how reliable is the two-strop

suspension as compared to the three-point suspension; is the pilot able to recover the helicopter when the front or the rear strop of the suspension system breaks, and, if yes, what are the limitations imposed to the flight envelope? The present paper investigates the responses of the helicopter and load suspended on a two- and three-point suspension when the front suspension point suddenly fails, determining whether the pilot is able to recover the helicopter.

The literature in this topic seems to be somewhat sparse. Many relevant publications relate more to the modelling of the dynamics of a helicopter with slung load (see refs. [2] and [4]). A few publications have been located but they address a rather different problem from that considered here, i.e. the situation in which a load is moving within an aircraft before being dropped (see refs. [3] and [1]).

The present work describes a multitude of failure scenarios of the front and back suspensions and determines the cases in which the redundant HUSLE can be eliminated. The paper is structured as follows:

- The first section develops a non-linear piloted simulation model representing the flight dynamics of a Chinook CH47-B helicopter carrying a suspended load in inverted V-suspension. The helicopter model includes six degree-of-freedom (6-dof) rigid body dynamics plus the dynamic inflow of both rotors included in the model as “quasi-dynamic” variables by means of time constants. To fly the helicopter, a pilot model is added to the 6-dof model in the form of a PID controller representing four stabilization functions for each control – longitudinal, collective, lateral and pedal. A 6-dof load model can be also connected to the helicopter model by means of slings hanging in two or three points.
- The second section presents the trim validation of the model for the clean helicopter and for the helicopter plus load system;
- The third section simulates different failure scenarios and determines the cases for safe manoeuvring with a two-and-three point suspension;
- Finally, general conclusions and potential future extension of this work are discussed.

Generic Six Degree-of-Freedom Model for Tandem Helicopters

Model description A general six degree-of-freedom (6-dof) non-linear rigid body model for a generic tandem helicopter was first developed for piloted simulations. This model was based on the generic single rotor

helicopter model developed at The Delft University [6]. In a typical 6-dof model, the helicopter is modelled by dividing it into main components (front rotor, rear rotor, fuselage, horizontal stabilizer, vertical fin) and summing up the contribution of each part to the general system of forces and moments. The following assumptions were made:

- Aerodynamic forces and moments are calculated using the blade element theory and integrating along the radius and azimuth to obtain their average effect;
- The fuselage is modelled with linear aerodynamics;
- Rotor disc-tilt dynamics (often the so-called ‘flapping dynamics’) is neglected and only steady-state rotor disc-tilt motion is considered;
- The dynamic inflow of both front and rear rotor are included in the model as state variables and can be described as a quasi-steady dynamic inflow by means of time constants of a value 0.1 sec;
- The rotors are modelled with a centrally flapping hinge;
- No pre-twist or pitch flap coupling are included;
- The lead-lag motion of the blades is neglected;
- The blades are rectangular;
- There are no pitch-flap or pitch-lag couplings;
- There are no tip losses;
- Gravitational forces are small compared to aerodynamic, inertial and centrifugal forces;
- The flapping and flow angles are small;
- The front rotor angular velocity is constant and anticlockwise, the rear rotor angular velocity is constant and clockwise;
- No reverse flow regions are considered;
- The flow is incompressible;
- The blades have a uniform mass distribution;
- The blade elastic axis, aerodynamic axis, control axis and centre of mass axis coincide.

The following sign conventions were used in the model:

- Longitudinal disc tilt for front and rear rotors a_{1f} and a_{1r} are assumed positive for backward tilted rotor disc plane;
- Lateral disc tilt for front and rear rotor b_{1f} and b_{1r} are positive for rotor disc plane tilted in the direction of azimuth angle $\psi=90^\circ$ (i.e. $b_{1f} > 0$ to the right and $b_{1r} > 0$ to the left, backside view);
- Collective pitch for front and rear rotor θ_{0f} and θ_{0r} are positive when the pilot moves the collective up;
- Longitudinal cyclic for front and rear rotor θ_{1sf} and θ_{1sr} are assumed positive when the pilot moves the stick forward;

- Lateral cyclic for front and rear rotors θ_{1cf} and θ_{1cr} are assumed positive when the pilot moves the stick to the right for cyclic pitch to the right.

For a complete derivation of the forces and moments acting on the helicopter components, the reader is referred to [7]. The equations of motion describing the motion of the helicopter in the 6-dof model are presented in Appendix A. To this model, a 6-dof model for the load has been added. The load is attached to the helicopter with slings modelled as linear weightless springs by means of a small internal damping.

To fly the helicopter, a pilot model is connected to the 6-dof model first at the level of stabilization and then at the level of guidance. The stabilisation level is the lowest level of pilot controlling because it is done unconsciously. This level consists in PID controllers that generate all control positions. The guidance level is the next higher level of controlling which allows the artificial pilot to achieve a wished speed or position. Actually, at this level the pilot becomes 'conscious' of his/her actions in the required parameters for executing a mission. The highest level of controlling, the so-called 'conscious level' is the navigation level. This level has not been implemented in the paper as no specific mission was investigated. Next section presents trim validations of the 6-dof model for the clean helicopter and helicopter+load system. Then, the validated model is used to fly different load failure scenarios.

Trim Results

Trim of the Clean Helicopter First, the 6-dof generic tandem helicopter model was validated for a Chinook CH-47B against a reference model developed in ref. 5 matching the flight test data of a Chinook CH-47B. Fig. 2 presents the validated pilot controls for the trimmed flight. For collective one may observe an underprediction of about 9% throughout the whole speed range. This may be explained by the level of modelling employed in the paper, where the use of simple momentum theory in accounting the fuselage download effects may have resulted in an underprediction of the induced power.

Fig. 3 presents the pitch and roll attitude for trimmed flight. One may observe that pitch attitude agrees quite well with the reference data, for the bank angle a difference of 20% or even more can be read over the whole velocity range. This error can be attributed to a more powerful effect of the non-uniform inflow on rotor flapping than it is assumed in the paper.

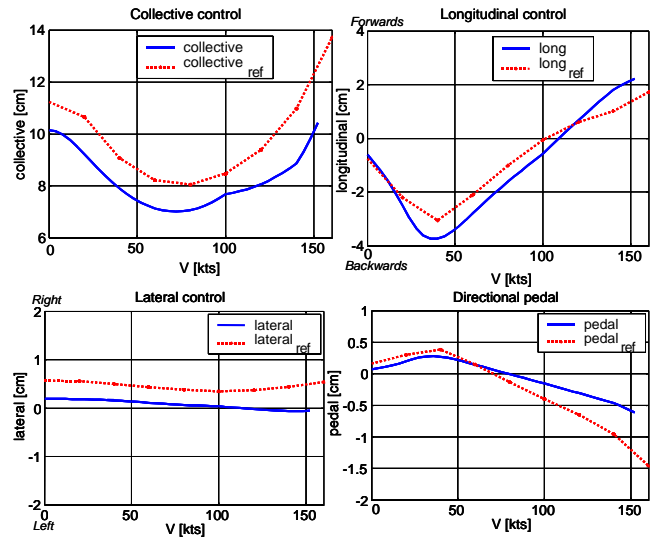


Fig. 2: Pilot controls for trimmed flight. Clean helicopter

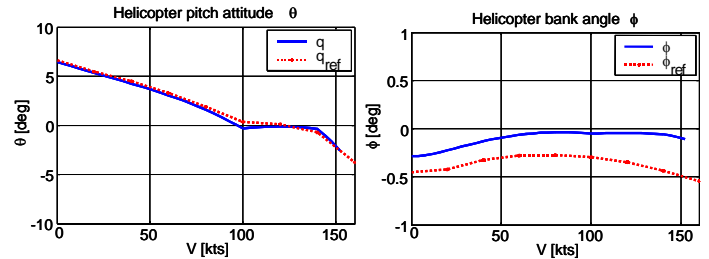


Fig. 3: Pitch and roll attitude in trimmed flight. Clean helicopter

Trim of the Helicopter with External Load The helicopter with external load is basically trimmed with the same method as the clean helicopter. In practice it appeared that trimming the helicopter + load at once didn't produce any solution. Therefore the load and the helicopter were trimmed separately. First, the load is trimmed assuming that the helicopter attitude angles equal zero, then a helicopter trim run is done with the cable forces of the load trim. This procedure is repeated with the new helicopter attitude for the load trim. Finally, the trim of the helicopter + load is determined in a new trim routine with states and controls of both bodies together. Fig. 4 presents the pilot controls for the trimmed flight of the helicopter carrying different external weights -2000, 6000 and 10000 kg. As expected, one needs more collective to transport a heavier load. Over 40 kts longitudinal cyclic must be increased as more weight is carried. Also, during the whole flight regime, heavier load means more stick to the right. At low flight velocities, more left pedal has to be applied.

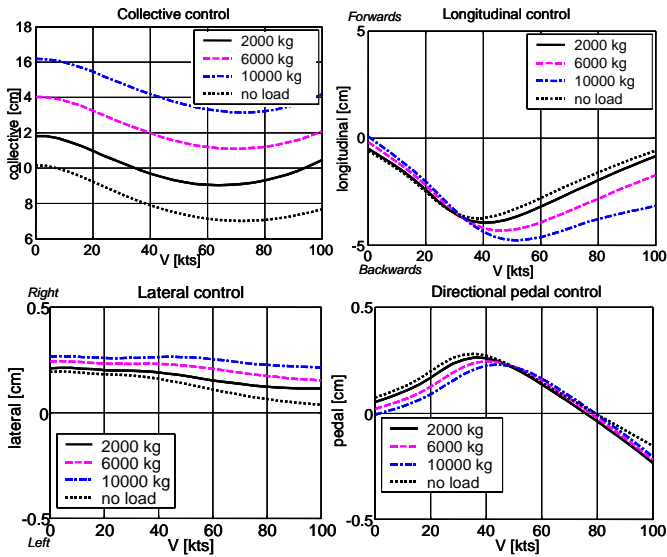


Fig. 4: Pilot controls for trimmed flight. Helicopter with external load

Fig. 5 presents the helicopter+load trim results. Compared to the unloaded flight, flying with the load at high velocities results in pitching nose-down of the helicopter, this as a result of the increased drag from the container transported underneath. As concerns the load position, looking at Fig. 5 one can read about the same attitude of the load as for the helicopter.

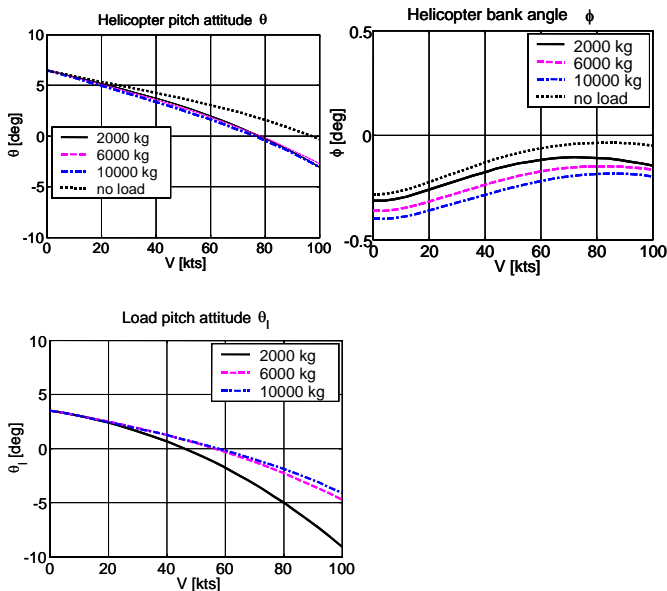


Fig. 5: Pitch and bank angles for trimmed flight; Helicopter+load trimmed system

Piloted Simulation of Different Cable Failure Scenarios

Failure of Front Cable The 6-dof model developed and validated in the previous paragraphs is used to simulate different failure scenarios of one of its cables. It is assumed that the failure of the cables at the rear hook is less dangerous than the failure of the cables at the front hook (this assumption will be confirmed later by simulations). The paper presents first the failure of the cables at the front suspension point. A tandem V-shape suspended load is assumed to hang underneath the helicopter so that failure of the front hook means actually failure of the two front cables (see Fig. A4). Two cases are investigated: 1) the load is suspended on two-point suspension system and 2) the load is suspended on three-point suspension system with the redundant set of slings (between the front and rear hook) coming into action when the front cables fail. In each case it is assumed that the load can be suspended either in a nose-down position (so-called 'nose-down rigged load') or in a horizontal position (so-called 'level rigged load'). As initial condition, it is considered that the helicopter is flying in forward flight at velocities varying between 10 and 100 kts and carries a container of 2000 kg, 6000 kg or 10000 kg. In the simulated failure scenarios, it is assumed that the pilot reaction time varies from instantaneously reaction (ideal case) to a delay in response of 1 and 2 seconds. To determine the limits within which the pilot can control the recovery, the ADS-33 standard [8] is used. Table 1 gives the Level 1 handling limits for large-amplitude attitude changes in hover and low speed flight (<45 kts) for aggressive agility manoeuvres. In forward flight (>45 kts), ADS-33 is qualitative in terms of achievable pitch rate and attitude angle where no limits are given. The present study considered that the same limits of Table 1 are valid for recovering from cable failure in forward flight.

Table 1: Level 1 ADS-33 requirements for large-amplitude changes - hover and low speed

Angular rates [deg/s]		Attitude angles [deg]	
p	± 50	ϕ	± 30
q	± 30	θ	± 30
r	± 60		

A typical failure simulation can be seen in Fig. 6. The case considered is the helicopter flying forward at 50 kts when a front failure occurs with a 2-point suspended load of 2000 kg. It is considered that the pilot reacts 1 sec after the failure. The controls remain unchanged from the moment of failure to the moment of pilot reaction (i.e. for 1 second).

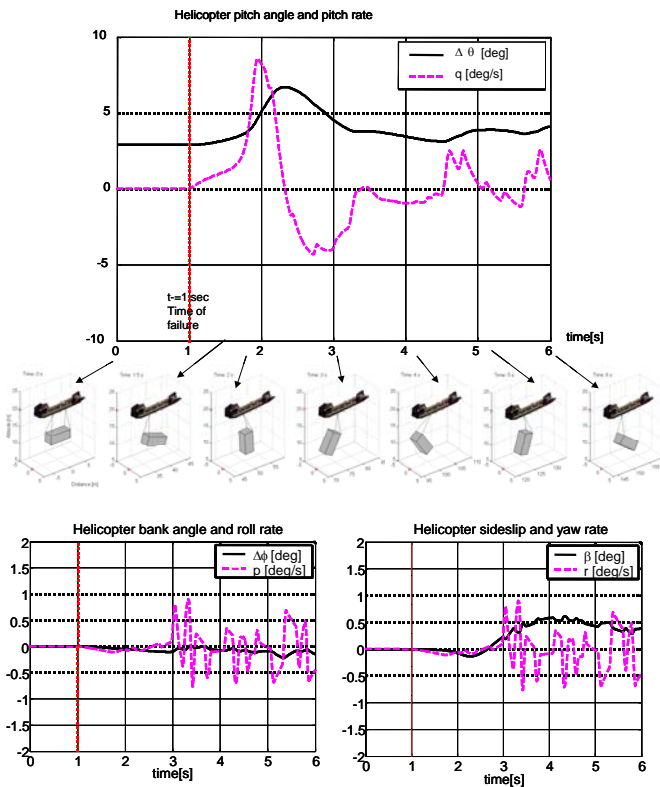


Fig. 6 Helicopter responses to a front cable failure scenario from 50 kts initial velocity, 2-point suspension, 2000 kg load, 1 sec delay in pilot reaction

Looking at Fig. 6 one could read a pitch rate of 10 deg/sec combined with some rolling and yawing when the load fails.

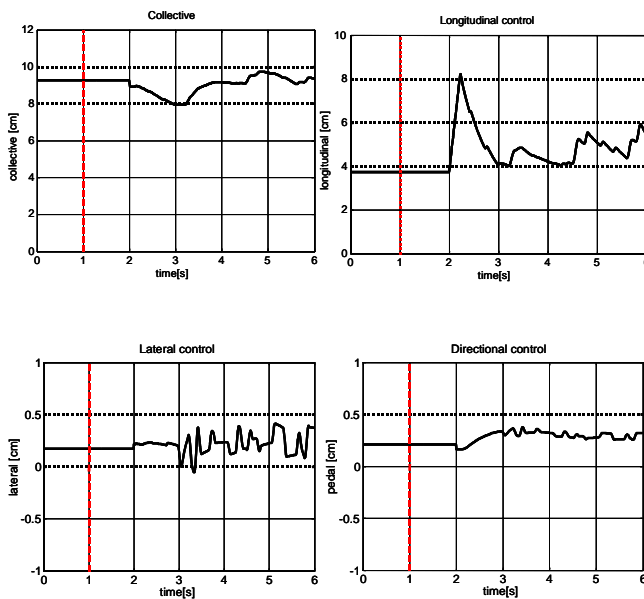


Fig. 7 Pilot controls after cable failure

From the simulation of the pilot controls it appears that the pilot can control this failure, his/her controls being plotted in Fig. 7.

Table 2(a) and (b) summarize the results obtained after simulating different failure scenarios of the front cable of a level-rigged load of different weights (2000 kg, 6000 kg, 10000 kg) suspended on a helicopter flying forward at velocities varying between 10 and 100 kts (10 kts, 20 kts, 30 kts, ..., 100 kts). The simulations consider different values of the delay in pilot reaction (0 sec, 1 sec, 2 sec). Table 2(a) considers that the load is attached in 3-point suspension (redundant) and Table 2(b) the case of 2-point suspension. The results are plotted in percentages of flights that have recovered from all 10 different scenarios considered of velocities varying between 10 kts and 100 kts (for example, 80% means that from 10 simulated failures, 8 have recovered).

Table 2 Chance to recover after a failure of the front-point suspension, level rigged load, non-snapping cables

(a) Case of 3-point suspension (redundant sling)

Load weight Pilot delay	2000kg redundant	6000 kg redundant	10000kg redundant
0 sec	100%	100%	100%
1 sec	100%	100%	90%
2 sec	100%	60%	50%

(b) Case of 2-point suspension

Load weight Pilot delay	2000kg	6000 kg	10000kg
0 sec	100%	100%	100%
1 sec	80%	80%	0%
2 sec	70%	0%	0%

Comparing Table 2(a) and 2(b), one can see that cable failure in 2-point suspension system can be fatal if the pilot does not react immediately, especially when the helicopter is transporting heavy loads. Considering that a normal pilot has a delay of maximum 2 second in reacting to the failure it means that eliminating the redundant sling is not a safe solution for flying with loads higher than 2000 kg.

It is interesting to determine the degradation in handling qualities characteristics when using a 2-point and a 3-point suspension. To investigate this problem, the pitch attitude quickness criterion as defined by the ADS-33 ([8], pp. 12) is explored. Pitch axis is chosen because the pitch motion is the largest motion after a load failure. The ADS-33 Levels 1/2/3 HQs of a general

task manoeuvre are considered. The attitude quickness parameter Q_θ in the ADS-33 is defined as the ratio of the maximum pitch rate q_{pk} to the peak attitude angle change $\Delta\theta_{pk}$, that is:

$$Q_\theta \stackrel{def}{=} \frac{q_{pk}}{\Delta\theta_{pk}} \text{ (sec}^{-1}\text{)} \quad (1)$$

ADS-33 defines level 1, 2 and 3 handling qualities for the attitude quickness parameter as a function of the minimum attitude change $\Delta\theta_{min}$. Fig. 8(a), (b) and (c) present the attitude quickness charts for the failure scenarios analysed. The ADS-33 level 1/2 and 2/3 boundaries for a target acquisition and tracking mission are also plotted in order to give the impression how the quickness in investigated failure scenarios are situated with respect to the ADS-33 levels.

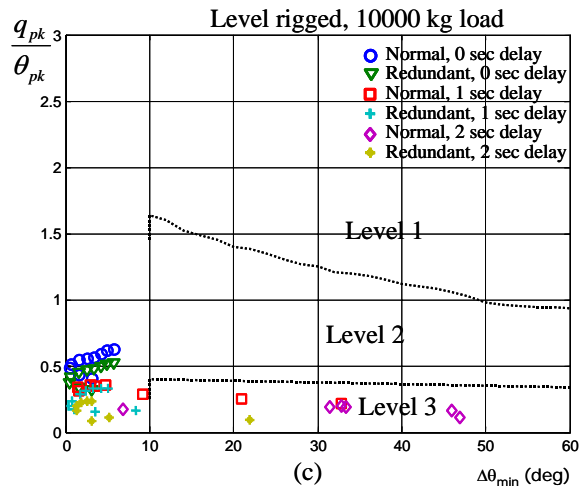
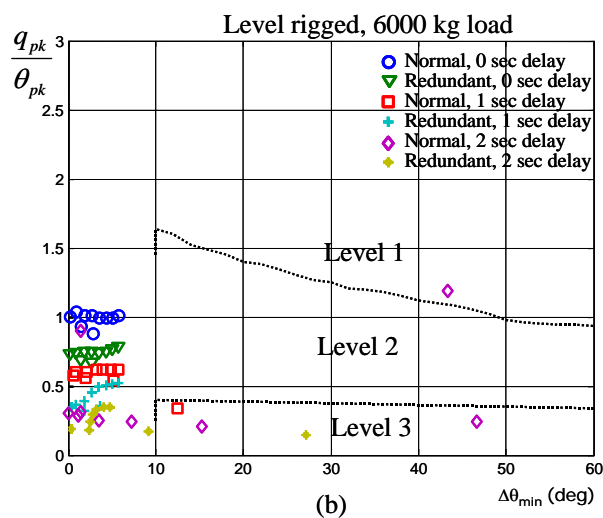
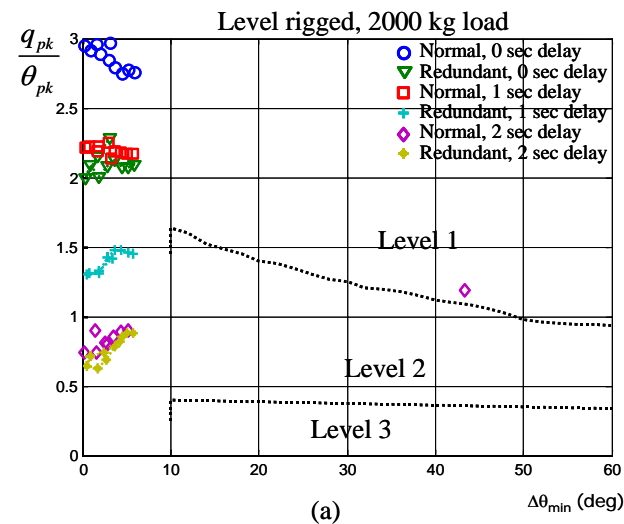


Fig. 8 Attitude quickness in pitch: front cable failure, normal and redundant configuration; different pilot time delays, level rigged load, non-snapping cables (a) 2000 kg load; (b) 6000 kg load; (c) 10000 kg load

Looking at this figure it becomes visible that carrying a heavier load results in quick degradation in handling qualities. The quickness when carrying the load in a 2-point suspension is higher than when carrying the load in 3-point suspension. This can be explained when thinking at the meaning of agility on the quickness charts. One has to realise that the more closer the pilot flies to the limit of performance envelope, the higher it becomes the value of the agility quickness achieved. Flying with two-point suspension results in more aggressive manoeuvring and thus gives more quickness to the pilot in changing the pitch. However, there is a kind of inverse trend between the agility achieved and the HQs ratings: increasing agility results in degradation the HQs ratings as the workload increases. Therefore one can expect that when flying with a 2-point suspension the pilots will return poorer HQs ratings than in the case of 3-point suspension. This judgment will have to be checked in the future work by performing piloted trials in full-motion simulators.

Different simulations have also been undertaken when the load was suspended nose-down. It was observed that, in this case, the chance to recover was higher than in the case of level rigged load either with a 2-point or a 3-point suspension system. However, as in the case of level rigged load, it could be concluded that for loads higher than 2000 kg it was advisable to still use the 3-point suspension.

Snapping of the remaining slings Analysing the pilot recovery chances after a front cable failure without dropping the external load, the following question came

to discussion: what happens if the remaining cables are not strong enough to carry the load and they will snap so that the pilot will loose anyway the load. Therefore the tension in the remaining cables was analysed to determine the cases in which the pilot would anyway loose the load. After a front cable failure the tension in the remaining cable(s) increases exponentially and may cause snapping of the other cable(s). The snapping of the other cables may cause extra piloting problems and even loss of control. For the 50 kts case analysed in Fig. 6, the forces in the remaining rear slings are represented in Fig. 9 (S21 right back sling, S22 left back sling). Looking at this figure one can see that the tension forces are rapidly increasing to values ten times higher than before the failure.

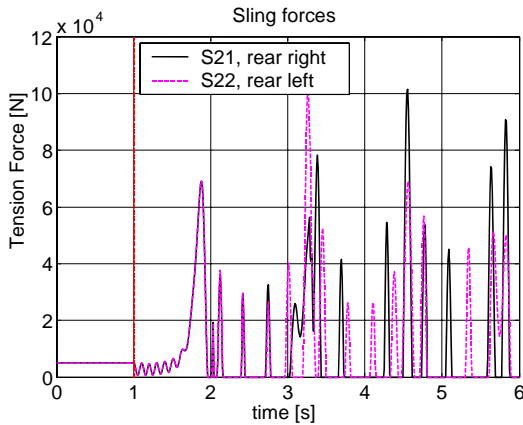


Fig. 9: Tension forces in the back slings after a 2-point cable failure

Table 3 summarizes the results obtained when simulating different scenarios as chance to recover when considering the risk of snapping cables. As sling specifications it is considered that the begin-of-life factor is 7 times the design load and end-of-life strength factor is 4.2. It is assumed that the slings snap when the begin-of-life is reached.

Table 3 Chance for recovering after a failure of the front-point suspension, level rigged load, snapping cables

(a) Case of 3-point suspension (redundant sling)

Load weight Pilot delay	2000 kg redundant	6000 kg redundant	10000 kg redundant
0 sec	100%	100%	100%
1 sec	100%	100%	90%
2 sec	100%	60%	50%

(b) Case of 2-point suspension

Load weight Pilot delay	2000kg	6000 kg	10000kg
0 sec	100%	100%	100%
1 sec	100%	80%	60%
2 sec	90%	0%	0%

Concerning the 3-point suspension, it is known that the redundant HUSLE is made of a less stiff material as compared to a normal sling, this in order to absorb the failure shock and prevent the load of large motions after failure. However, this makes the redundant sling even more expensive than a normal sling. Therefore, the following question was posed: is the redundant HUSLE strong enough to resist snapping and what if it would be made from the same material as the normal sling to reduce costs?

The results showed that for the 2000 kg load it does not really matter what material is used for the HUSLE; for the 6000 and 10000kg, changing the HUSLE material from a low to a high stiffness material, results in premature snapping. It can be concluded that using low stiffness material for redundant sling is an important aspect that cannot be changed.

Failure of Rear Cable Finally, failures of the rear cable were analysed. Table 4 (a) and (b) summarize the results obtained after simulating the failure of the rear cable of a 3-point and a 2-point level rigged load of different weights when the helicopter is flying at different initial velocities and there is 0, 1 and 2 second delay in pilot reaction to the failure. The results are given in percentages of flights that have recovered. One can see that flying the 10000 kg load with a 2-point suspension is fatal for all velocities (10 to 100 kts) when the pilot delays more than 1 second to react to the failure. Using the redundant load improves noticeably the results, resulting in a 50% chance to recover of the 10000 kg weight. Comparing Table 4(a), (b) for rear cable failures with Table 2(a), (b) for front cable failures, one can see that rear cable failure is a bit less dangerous than front cable failure as the chance to recover from a rear cable failure is higher than one of front cable failure.

Table 4: Chance for recovering after a failure of the rear-point suspension, level rigged load, non-snapping cables

(a) Case of 3-point suspension (redundant sling)

Load weight Pilot delay	2000 kg redundant	6000 kg redundant	10000 kg redundant
0 sec	100%	100%	100%
1 sec	100%	100%	100%
2 sec	100%	70%	50%

(b) 2-point suspension (redundant sling)

Load weight	2000 kg	6000 kg	10000 kg
Pilot delay			
0 sec	100%	100%	100%
1 sec	100%	100%	0%
2 sec	100%	0%	0%

Fig. 10(a), (b) and (c) present the attitude quickness charts for rear cable failures plotted in ADS-33 level 1/2 and 2/3 boundaries of a target and acquisition and tracking mission. Comparing Fig. 10 with Fig. 8, one can see that rear failure of a 2000 kg is not depending very much on the pilot delay in reaction to the failure, the HQs corresponding to Level 2 HQs.

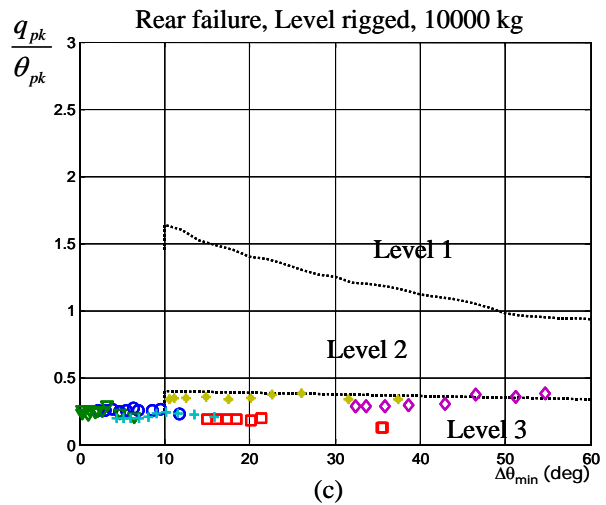
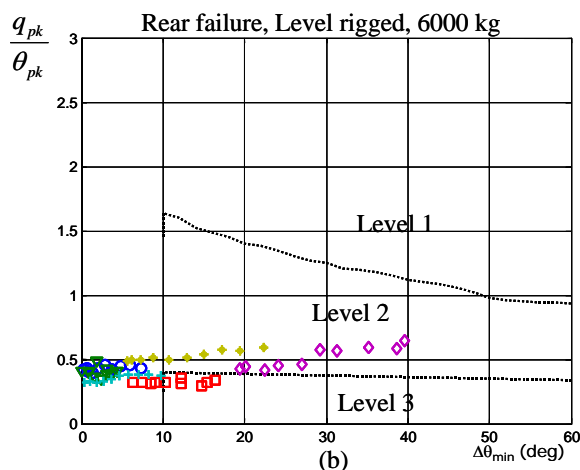
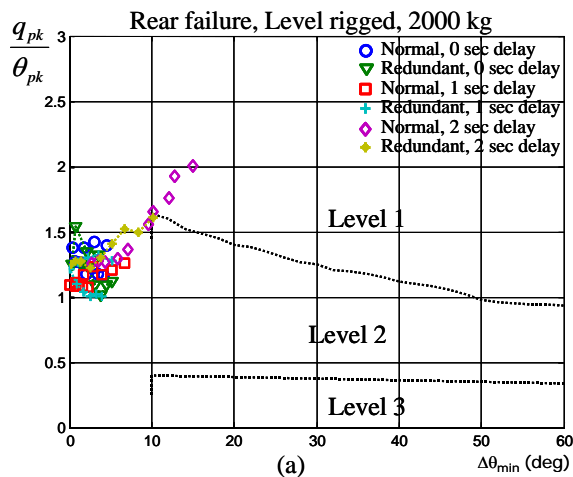


Fig. 10: Attitude quickness in pitch for rear cable failure of a load in normal and redundant configuration, different pilot delays, level rigged load, non-snapping cables. (a) 2000 kg; (b) 6000 kg (c) 10000 kg

Also, one can see that, from HQs point of view, rear cable failure is as difficult to fly as the front cable failure.

Conclusions and Future Work

The exercise of this paper was to determine for a Chinook helicopter with external slung load whether it was safely enough to replace the three-point suspension system by a two-point suspension system and eliminate the redundant HUSLE. A generic six degree-of-freedom non-linear model was developed for the helicopter and combined with a 6-dof load model, the helicopter controls being modelled in a pilot model at the level of stabilization with PID controllers. Trim validation of the clean helicopter against a NASA model from the literature of speciality proved good agreements. The paper analysed a multitude of scenarios following the premature breakdown of one of the cables sustaining the slung load – forward flight velocities between 10 and 100 kts, level and nose-down rigged load, snapping and non-snapping slings, pilot delay in reaction of 0, 1 and 2 second – and determined when the pilot could recover or not. It was concluded that for light containers of up to 2000 kg, the 3-point suspension could be replaced by the 2-point suspension, no matter how much delay was in the pilot reaction to the failure. However, for 6000 and 10000kg containers the use of the 2-point suspension resulted in increasing the probability to lose the control and crush provided that the pilot didn't drop the load on time. This conclusion was especially true when the pilot delay was high (2 sec). Analysing the possibility of the remaining cables to snap it could be concluded that

at high loads (10000kg) and high velocities (70-100kts) the remaining cable of the 2-point suspension snapped and the load was lost. However, in these cases the load had to be dropped anyway as the pilot could not control the helicopter. The redundant HUSLE in the 3-point suspension is made of a low stiff material and it is recommended to not change this property, as a higher stiffness redundant HUSLE would not absorb enough from the failure shock, making the use of redundant cable superfluous. Analysing rear cable failures showed a bit higher probability in recovering. Finally, from the cases analysed it could be concluded that flying with the nose-down rigged load was less dangerous than flying with the level-rigged load. As expected, analysing the HQs characteristics in premature failures as given by the pitch attitude quickness criterion, a quick degradation in HQs was obtained when the pilot had a delay in reaction of more than 1 second.

The work presented in this paper will be extended in the future to a larger database of situations. Also, a higher level of sophistication in the pilot model will be implemented in the form of the a full AFCS, this in order to ensure the validity of the results for the RNLA operations with Chinooks.

References

1. Bernstein, L., "On the equations of Motion for an Aircraft with an Internal Moving Load which is then Dropped", Aeronautical J., Vol. 102, No., 1011, Jan. 1998, pp. 9-24
2. Cicolani, Luigi S., et.al., "Simulation of the Dynamics of Helicopter Slung Load Systems", J. of the American Helicopter Society, Vol. 40, No. 4, October 1995, pp. 44-61
3. Dzygadło, Z., Sibilski, K., "Dynamics of longitudinal motion of an aeroplane after drop of loads", J. Tech. Phys, Vol. 28, No. 3, 1987, pp. 365-373
4. Fusato, Dario, et. al., "Flight Dynamics of an Articulated Rotor Helicopter with an External Load", J. of the American Helicopter Society, Vol. 46, No. 1, January 2001, pp. 3-12
5. Ostroff A.J., D.R. Downing, W.J. Rood, "A technique using a non-linear helicopter model for determining trims and derivatives", NASA TN D-8159, Langley Research Center Hampton, Va, May 1976

6. Pavel, Marilena D., "On the Necessary Degrees of Freedom for Helicopter and Wind Turbine Low-Frequency Mode-Modelling", Ph.D. Dissertation, Delft University of Technology, 2001
7. Reinier van der Kamp, "Investigation on the Chinook Operations with an External Tandem Load after Cable Failure", Graduation Report TU Delft, June 2005
8. anon., Aeronautical Design Standard-33E-PRF, Performance Specification, Handling Qualities Requirements for Military Rotorcraft, US Army AMCOM, Redstone, Alabama, March 21, 2000.

Appendix A

Derivation of the equations of motion in a six degree-of-freedom model In a general 6-dof non-linear body model the helicopter motion is represented by three translations and three rotations around the body axes-system $\bar{E}_B \{X_B Y_B Z_B\}$ centred in the helicopter centre of gravity, see Fig. A 1.

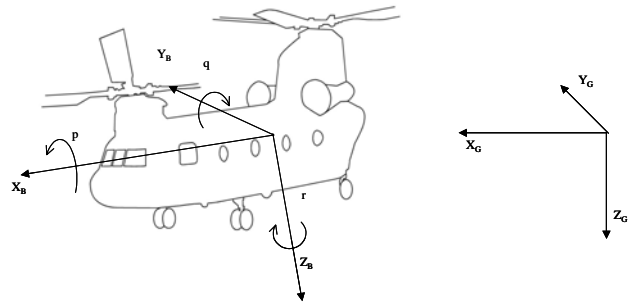


Fig. A 1: System of coordinates used to express the helicopter motion in the 6-dof model

The system of equations describing completely the motion of the helicopter in an inertial system are:

$$\begin{aligned}
 \dot{u} &= -g \sin \theta + \frac{X}{m} + rv - qw \\
 \dot{v} &= g \sin \phi \cos \theta + \frac{Y}{m} - ru + pw \\
 \dot{w} &= g \cos \phi \cos \theta + \frac{Z}{m} + qu - pv \\
 \dot{p} &= \frac{rqI_3 - pqI_{xy}I_z + I_zL + I_{xz}N}{I_1} \\
 \dot{q} &= \frac{M + pr(I_z - I_x) + I_{xz}(r^2 - p^2)}{I_y} \\
 \dot{r} &= \frac{-rqI_{xz}I_2 + pqI_4 + I_{xz}L + I_xN}{I_1}
 \end{aligned} \tag{2}$$

$$\dot{\psi} = \frac{(q \sin \phi + r \cos \phi)}{\cos \theta}$$

$$\dot{\theta} = q \cos \phi - r \sin \phi$$

$$\dot{\phi} = p + \dot{\psi} \sin \theta$$

with $I_1 = I_x I_z - I_{xz}^2$, $I_2 = I_x - I_y + I_z$, $I_3 = I_y I_z - I_z^2 - I_{xz}^2$, $I_4 = I_x^2 - I_x I_y + I_{xz}^2$. In order to describe completely the helicopter motion w.r.t. the Earth system, the equations of trajectory can be added:

$$\begin{aligned} \dot{x} &= (u \cos \theta + (v \sin \phi + w \cos \phi) \sin \theta) \cos \psi - (v \cos \phi - w \sin \phi) \sin \psi \\ \dot{y} &= (u \cos \theta + (v \sin \phi + w \cos \phi) \sin \theta) \sin \psi + (v \cos \phi - w \sin \phi) \cos \psi \\ \dot{z} &= -u \sin \theta + (v \sin \phi + w \cos \phi) \cos \theta \end{aligned} \quad (3)$$

To these systems of equations, two differential equations are added for the dynamic inflow of the front main and rear rotors, describing the dynamic inflow as a “quasi-steady inflow” by means of time constants:

$$\tau_f \dot{\lambda}_f = C_{T,Elem,f} - C_{T,Glau,f}$$

$$\tau_r \dot{\lambda}_r = C_{T,Elem,r} - C_{T,Glau,r} \quad (4)$$

where $C_{T,elem}$ and $C_{T,Glau}$ are the rotors thrust coefficients as expressed in blade element theory and respectively Glauert theory.

The total forces and moments acting on the helicopter centre of gravity consist of the sum of front and rear rotor (with indices Rf and Rr), rotor torque (Q) and helicopter body aerodynamics (B). For the load, a suspension point component (S) is considered which is added when the load is attached underneath the helicopter model.

$$\begin{aligned} X &= X_{Rf} + X_{Rr} + X_B (+X_S) \\ Y &= Y_{Rf} + Y_{Rr} + Y_B (+Y_S) \\ Z &= Z_{Rf} + Z_{Rr} + Z_B (+Z_S) \\ L &= L_{Qf} + L_{Qr} + L_{Rf} + L_{Rr} + L_B (+L_S) \\ M &= M_{Rf} + M_{Rr} + M_B (+M_S) \\ N &= N_{Qf} + N_{Qr} + N_{Rf} + N_{Rr} + N_B (+N_S) \end{aligned} \quad (5)$$

The rotor forces and moments are consisting of front and rear vertical thrust components T_f and T_r , drag forces H_{Xf} and H_{Xr} , lateral forces H_{Yf} , and H_{Yr} and rotor shaft torques M_{Qf} and M_{Qr} as seen in Fig. A 2.

$$\begin{aligned} X_{Rf} &= X_{Tf} + X_{Hf} & X_{Rr} &= X_{Tr} + X_{Hr} \\ Y_{Rf} &= Y_{Tf} + Y_{Hf} & Y_{Rr} &= Y_{Tr} + Y_{Hr} \\ Z_{Rf} &= Z_{Tf} + Z_{Hf} & Z_{Rr} &= Z_{Tr} + Z_{Hr} \\ L_{Rf} &= Y_{Rf} h_f - Z_{Rf} f_1 + L_{Qf} & L_{Rr} &= Y_{Rr} h_r - Z_{Rr} f_1 + L_{Qr} \\ M_{Rf} &= -X_{Rf} h_f - Z_{Rf} l_f & M_{Rr} &= -X_{Rr} h_r + Z_{Rr} l_r \\ N_{Rf} &= X_{Rf} f_1 + Y_{Rf} l_f + N_{Qf} & N_{Rr} &= X_{Rr} f_1 - Y_{Rr} l_r + N_{Qr} \end{aligned} \quad (6)$$

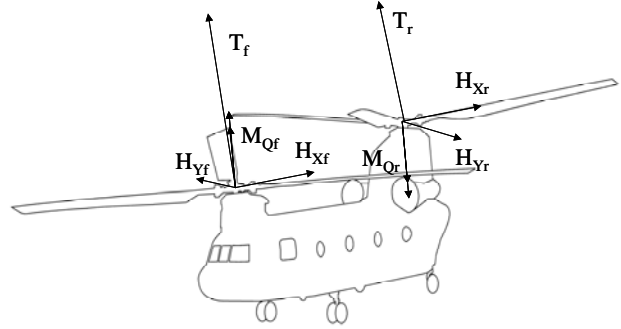


Fig. A 2: Forces and Moments on the rotors

The contributions of these components to the front rotor thrust and the horizontal and side forces in the helicopter body system are:

$$\begin{aligned} X_{Tf} &= T_f \sin(\theta_{1sf} - a_{1f} + i_f) \cos(\theta_{1cf} + b_{1f}) \\ X_{Hf} &= -H_{Xf} \cos(\theta_{1sf} - a_{1f} + i_f) - \\ &\quad - H_{Yf} \sin(\theta_{1cf} + b_{1f}) \sin(\theta_{1sf} - a_{1f} + i_f) \\ Y_{Tf} &= T_f \sin(\theta_{1cf} + b_{1f}) \cos(\theta_{1sf} - a_{1f} + i_f) \\ Y_{Hf} &= H_{Yf} \cos(\theta_{1cf} + b_{1f}) \\ Z_{Tf} &= -T_f \cos(\theta_{1sf} - a_{1f} + i_f) \cos(\theta_{1cf} + b_{1f}) \\ Z_{Hf} &= -H_{Xf} \sin(\theta_{1sf} - a_{1f} + i_f) + \\ &\quad + H_{Yf} \sin(\theta_{1cf} + b_{1f}) \sin(\theta_{1sf} - a_{1f} + i_f) \\ L_{Qf} &= M_{Qf} \sin i_f \\ N_{Qf} &= -M_{Qf} \cos i_f \end{aligned} \quad (7)$$

For the rear rotor, these components are (note the opposite direction of the lateral flapping angle b_{1r} with respect to the front rotor equations):

$$\begin{aligned}
X_{Tr} &= T_r \sin(\theta_{1sr} - a_{1r} + i_r) \cos(\theta_{1cr} - b_{1r}) \\
X_{Hr} &= -H_{Xr} \cos(\theta_{1sr} - a_{1r} + i_r) \\
&\quad + H_{Yr} \sin(\theta_{1cr} - b_{1r}) \sin(\theta_{1sr} - a_{1r} + i_r) \\
Y_{Tr} &= T_r \sin(\theta_{1cr} - b_{1r}) \cos(\theta_{1sr} - a_{1r} + i_r) \\
Y_{Hr} &= -H_{Yr} \cos(\theta_{1cr} - b_{1r}) \\
Z_{Tr} &= -T_r \cos(\theta_{1sr} - a_{1r} + i_r) \cos(\theta_{1cr} - b_{1r}) \\
Z_{Hr} &= -H_{Xr} \sin(\theta_{1sr} - a_{1r} + i_r) - \\
&\quad - H_{Yr} \sin(\theta_{1cr} - b_{1r}) \cos(\theta_{1sr} - a_{1r} + i_r) \\
L_{Qr} &= -M_{Qr} \sin i_r \\
N_{Qr} &= M_{Qr} \cos i_r
\end{aligned} \tag{8}$$

The front and the rear rotor thrust, horizontal force (drag force) and lateral forces are calculated using the blade element theory by integration of the lift and drag forces on each blade element along the blade and around the azimuth (see the formulas in ref. [6], page 235). Their non-dimensional coefficients w.r.t. the disc plane (non-dimensionalized by $\rho(\Omega R)^2(\pi R^2)$) are:

$$C_T \approx C_{T,elem} = \frac{\sigma C_l^\alpha}{2} \left[\frac{\theta_0}{3} \left(1 + \frac{3}{2} \mu_x \right) + \frac{\mu_z - \lambda_0}{2} \right] \tag{9}$$

$$C_S = \frac{\sigma C_l^\alpha}{2} \left[\mu_x^2 \left(\frac{b_1 \theta_0}{2} - a_0 a_1 \right) + \mu_x \cdot \left(\frac{a_1 b_1}{4} + \frac{3 \lambda a_0}{2} - \frac{3 a_0 \theta_0}{4} \right) + \frac{\theta_0 b_1}{3} - \frac{3 \lambda b_1}{4} + \frac{a_0 a_1}{6} \right] - C_T b_1 \tag{10}$$

$$C_H = \frac{\sigma C_l^\alpha}{2} \left[\frac{\mu_x C_{dm}}{2 C_l^\alpha} + \theta_0 \left(\frac{a_1}{3} - \frac{\mu_x \mu_z - \lambda_0}{2} \right) + \frac{3(\mu_z - \lambda_0) a_1}{2} + \frac{\mu_x}{4} (a_0^2 + a_1^2) - \frac{a_0 b_1}{6} \right] - C_T a_1 \tag{11}$$

The main rotor thrust coefficient in Glauert theory is:

$$C_{T,Glauert} = 2 \lambda_0 \sqrt{\mu_x^2 + (\mu_z - \lambda_0)^2} \tag{12}$$

The rotor torque coefficient can be expressed as:

$$C_Q = \frac{\sigma}{8} C_d (1 + 4.7 \mu_x^2) + C_T \lambda_D - \mu_x C_H \tag{13}$$

The fuselage forces and moments are calculated through flat plate theory using ref. 5:

$$\begin{aligned}
X_B &= -C_{FE} \frac{1}{2} \rho V^2 \cos \alpha_{fus} \cos \beta_{fus} \\
Y_B &= -C_{Y\beta} \frac{1}{2} \rho V^2 \sin \beta_{fus} \\
Z_B &= -C_{L\alpha} \frac{1}{2} \rho V^2 \sin \alpha_{fus} \\
L_B &= -C_{L\beta} \frac{1}{2} \rho V^2 \sin \beta_{fus} |\cos \beta_{fus}| (1 - |\sin \alpha_{fus}|) \\
M_B &= C_{M\alpha} \frac{1}{2} \rho V^2 \sin \alpha_{fus} \cos \alpha_{fus} \\
N_B &= -C_{N\beta} \frac{1}{2} \rho V^2 \sin \beta_{fus} \cos \beta_{fus} (0.94 \sin \alpha_{fus} + 0.342 \cos \alpha_{fus})
\end{aligned} \tag{14}$$

The helicopter has three suspension points $i=1,2,3$ underneath its floor as seen in Fig. A3, the tension force in one cable j being S_{ij} .

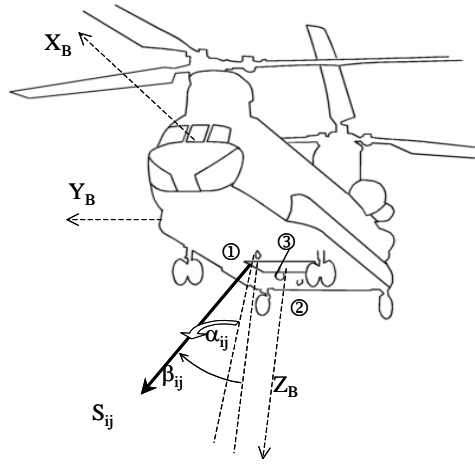


Fig. A3: Hooks and slings loads

The total forces on the slings are:

$$\begin{aligned}
X_S &= S_{ij} \cos \alpha_{ij} \sin \beta_{ij} \\
Y_S &= S_{ij} \sin \alpha_{ij} \sin \beta_{ij} \\
Z_S &= S_{ij} \cos \beta_{ij}
\end{aligned} \tag{15}$$

$$\begin{aligned}
L_S &= -S_{ij} \{ \sin \alpha_{ij} \sin \beta_{ij} h s_i - \cos \beta_{ij} f_i \} \\
M_S &= S_{ij} \cos \alpha_{ij} \sin \beta_{ij} h s_i - S_{1,3j} \cos \beta_{1,3j} f_{s_{1,3}} + S_{2j} \cos \beta_{2j} f_{s_2} \\
N_S &= S_{ij} \cos \alpha_{ij} \sin \beta_{ij} f_{i_1} + S_{1,3j} \sin \alpha_{1,3j} \sin \beta_{1,3j} f_{s_{1,3}} - S_{2j} \sin \alpha_{2j} \sin \beta_{2j} f_{s_2}
\end{aligned}$$

where α_{ij} and β_{ij} are the angles that the sling cable makes with the X and Z direction; $fs_{1,2,3}$ and $hs_{1,2,3}$ are the hook distances to the helicopter centre of gravity.

To fly the helicopter, a pilot model was introduced for stabilization of the helicopter motion in the form of a PID controller. Collective controls the altitude, longitudinal cyclic controls pitch attitude, lateral controls roll motion and pedal controls the sideslip:

$$\theta_0 = K_z (z_{req} - z) + K_{int_z} \int (z_{req} - z) dt + K_w w$$

$$\begin{aligned}
\theta_{1s} &= K_{\theta} (\theta_{req} - \theta) + K_{int_{\theta}} \int (\theta_{req} - \theta) dt + K_q q \\
\phi &= K_{\phi} (\phi_{req} - \phi) + K_{int_{\phi}} \int (\phi_{req} - \phi) dt + K_p p \\
\theta_{0p} &= -K_{\psi} \beta_{fus} + K_{int_{\psi}} \int (-\beta_{fus}) dt - K_r r
\end{aligned} \tag{16}$$

At the guidance level, the required pitch attitude is controlled by an altitude hold controller and the required roll angle is controlled by a lateral position hold controller.

$$\begin{aligned}
\theta_{req} &= K_{h1} (h_{req} - h) + K_{int_h} \int (h_{req} - h) dt + K_{hdot} \dot{h} \\
\phi_{req} &= K_y (y_{req} - y) + K_{int_y} \int (y_{req} - y) dt + K_{ydot} \dot{y}
\end{aligned} \tag{17}$$

The longitudinal and lateral pilot inputs are mixed at the level of swashplate as given in ref. 5.

$$\begin{aligned}
\theta_{1cf} &= \theta_{1cf,pilot} \cdot \cos \beta_{fus} + \theta_{1sf,pilot} \cdot \sin \beta_{fus} \\
\theta_{1sf} &= \theta_{1cf,pilot} \cdot \sin \beta_{fus} - \theta_{1sf,pilot} \cdot \cos \beta_{fus} \\
\theta_{1cr} &= \theta_{1cr,pilot} \cdot \cos \beta_{fus} + \theta_{1sr,pilot} \cdot \sin \beta_{fus} \\
\theta_{1sr} &= -\theta_{1cr,pilot} \cdot \sin \beta_{fus} + \theta_{1sr,pilot} \cdot \cos \beta_{fus}
\end{aligned} \tag{18}$$

Load model The load is modelled as a 6-dof body, the helicopter slings being connected to the load as seen in Fig. A4.

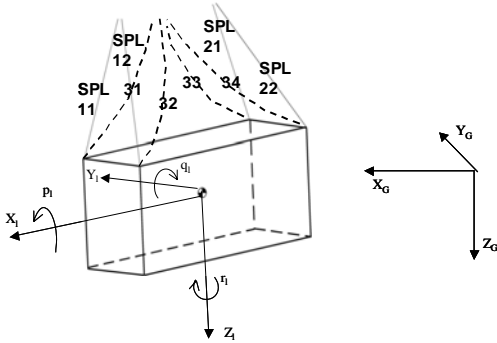


Fig. A4 Container load with local axes and sling numbering

For the derivation of the load model the reader is referred to ref. [7].